Fuel 322 (2022) 123936

Contents lists available at ScienceDirect

Fuel

journal homepage: www.elsevier.com/locate/fuel

Full Length Article

Ammonia injection failure diagnostic and correction in engine after-treatment system by NOx and NH3 emissions observation

Benjamín Pla, Pau Bares, Enrique José Sanchis, André Nakaema Aronis *

CMT-Motores Térmicos, Universitat Politècnica de València, Camino de Vera s/n, 46022 Valencia, Spain

ARTICLE INFO

Keywords:
Engine control
Fault detection diagnosis
Emissions control
Vehicle emissions

ABSTRACT

To ensure that after-treatment systems (ATS) reduce emissions to the levels for which they were designed, it is essential that the ATS control can rely on the feedback signals from the sensors and actuators that are part of the system. Knowing that the amount of ammonia injected into the catalyst governs the Nitrogen oxides (NOx) reduction, this work addresses the impact of the ammonia injection failure in the Selective Catalytic Reduction (SCR) on the exhaust emissions and describes a model-based fault diagnosis strategy. The proposed approach is based on an artificial neural network (ANN) and a sensor signal analysis (SSA) model of the catalyst, as well as an observer to merge the models and accurately estimate the emissions. The proposed diagnostic strategy is based on the comparison of the observed NOx and ammonia (NH3) emissions of the actual system with those expected in the system without ammonia injection failure. Experimental results show that the proposed strategy can detect failures in ammonia injection above 10%. Once the degradation level is detected, a correction strategy is applied by increasing the ammonia injector opening time according to the estimated degradation to increase the injected ammonia up to levels similar to faultless conditions. When the injection failure was corrected, the proposed strategy was able to mitigate the impact on NOx emissions, reducing them by 23.33% and approaching the NOx levels without injection failure (5.35% increase).

1. Introduction

Due to the impact of the internal combustion engine (ICE) exhaust emission on nature [1] and human health [2], the institutional and governmental appeal has grown [3] and the intrinsic production of Nitrogen oxides (NOx) emissions in the compression ignition combustion process, has become an important issue for diesel engines [4]. In this sense, emission standards have led ICE to be modified and significantly improved to increase efficiency and achieve ecological goals [5]. However, in order to improve ICE, new and complex systems were added, as well as sensors and control strategies were developed, consequently increasing the possibility of failures [6,7].

One of the systems added to achieve the emission limit objectives is the after-treatment systems (ATS). Regarding the NOx emissions, the most widely used is the Selective Catalytic Reduction (SCR), which is capable of reducing emissions by up to 95% through ammonia injection into the catalyst [8,9].

However, for the development of a reliable strategy to reduce NOx emissions, it is not only necessary to have a robust and efficient strategy but also to ensure that the actuators and sensors that feedback the information to the electronic control unit (ECU) work properly [10]. Therefore, fault detection and diagnosis in the peripheral systems of the ATS are of great importance and have a considerable impact on engine performance [11,12].

An example is a failure during the ammonia injector's life, where ammonia deposits usually appear, and the relation between the injector actuation and the ammonia flow can change with time as the engine ages [13,14]. As an example, Fig. 1 shows how an increase in the failure level of the ammonia injector leads to higher NOx emissions downstream of the SCR.

Understanding the importance of the subject, several authors have addressed techniques and strategies to monitor system failures over the past few years.

Vignesh and Ashok [14] did a review about the state-of-the-art of the SCR catalyst for De-NOx strategy, in the section dealing with failures, when it comes to the control unit faults, authors point out sensor measurement errors as the main failure for SCR control. When related to the reductant supply unit, the faults are due to deviations in ammonia injection, failure of the actuators, and progressive deposition of ammonia blocking the passage nozzle.

Mora et al. [15] proposed an On-Board Diagnostic (OBD) based strategy to detect catalyst ageing and ammonia injection failures. The fault approach uses an estimator that integrates a 400-seconds time

* Corresponding author.
E-mail address: annaar3@mot.upv.es (A. Nakaema Aronis).

https://doi.org/10.1016/j.fuel.2022.123936
Received 10 February 2022; Received in revised form 10 March 2022; Accepted 19 March 2022
Available online 14 April 2022

Nomenclature

Abbreviations

ANN	Artificial Neural Network
ASC	Ammonia Slip Catalyst
ATS	After-Treatment Systems
AWS	Accumulation Windows Size
ECU	Electronic Control Unit
EGR	Exhaust Gas Recirculation
EKF	Extended Kalman Filter
FTIR	Fourier-Transform Infrared Spectroscopy
ICE	Internal Combustion Engine
IF	Injection Factor
LNT	Lean NOx Trap
LS	Least Square
NEDC	European Driving Cycle
OBD	On-Board Diagnostics
RLS	Road Load Simulation
RTS	Standardized Random Test
SCR	Selective Catalytic Reduction
SCRF	Selective Catalytic Reduction Filter
SSA	Sensor Signal Analysis
VGT	Variable Geometry Turbine
WLTC	Worldwide harmonized Light vehicles Test Cycle

Symbols

K_{CS}	NO_x sensor cross sensitivity
$\dot{m}_{exh}$	Exhaust mass flow
NH_3	Ammonia
$NH_{3,inj}$	Ammonia injected into the SCR
NO_x	Nitrogen oxides
T_{SCR}	SCR catalyst temperature sensor
η_{NO_x}	SCR NO_x conversion efficiency

Superscripts

ds	Downstream
us	Upstream
thr	Threshold

horizon and compares the NOx and ammonia (NH3) measured and estimated. As a result, the methodology proved to be robust and can be used as feedback to improve control accuracy.

Canova et al. [16] created a model-based fault detection for a lean NOx trap (LNT) after-treatment system to detect and isolate the failures in the sensors and LNT parameters. The approach was capable of robustly and reliably detect critical faults such as sulphur poisoning, deactivation of catalyst storage due to thermal ageing, and sensor failures. Finally, it showed that the methodology can be extended to SCR and DPF systems.

Arsie et al. [17] created a virtual NOx sensor via an artificial neural network to estimate NOx emissions in a diesel engine and simulated a system failure that would affect the emission prediction, which can be accessed through the proposed least square-based (LS-based) algorithm. When submitted to a simulated failure, the LS-based system was able to estimate emissions with high accuracy, achieving a relative integral error index of 0.347% in a Hot New European Driving Cycle (Hot-NEDC) transient cycle.

Wang et al. [18] created a fault detection and fault tolerant control of the urea injection system, the proposed strategy uses the line

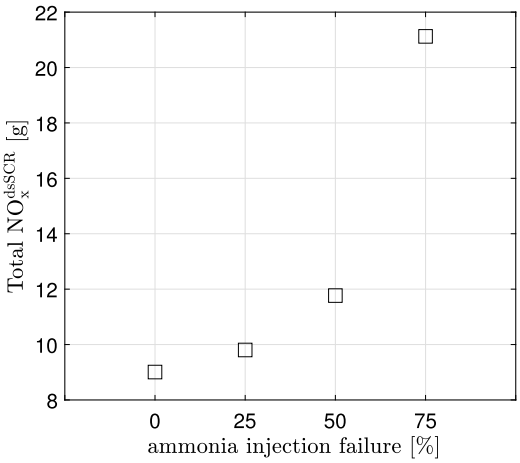

Fig. 1. Increase in total NOx emissions downstream of the SCR catalyst with the increased failure of ammonia injection in a Worldwide harmonized Light vehicles Test Cycle (WLTC) cycle (i.e., the data was acquired experimentally simulating an error in the ammonia injection, for each case the % is in relation to the nominal amount of ammonia demanded by the system).

pressure sensor feedback combined with a Kalman filter to estimate the actual effective area of the urea injector orifice, thus the ratio of current and expected effective area is used to compensate the line pressure. As a result, the proposed methodology was able to detect and correct an injection failure when the dosage falls below 80%.

Failures in feedback signals can compromise the correct behaviour of the entire ATS, in the case of the SCR catalyst, the SCR control unit is responsible for the supply of the reducing agent (ammonia), furthermore, detecting ammonia under or overdosage is a current requirement of European OBD regulations [14]. A failure in the feedback signal from the sensors and/or actuators affects the ammonia dosage, generating a supply rate different from that required, leading to an inefficient NOx conversion rate. The impact on ammonia supply is highly damaging as it reduces the performance of harmful gases converted before they are released into the environment.

Therefore, this work aims to contribute with a novel methodology to detect ammonia injection failure in the SCR catalyst and correct it, avoiding a reduction in the catalyst's conversion efficiency rate and, consequently, an increase in NOx and NH3 emissions. The approach combined control-oriented models and data fusion techniques, such as the extended Kalman filter (EKF), to accurately predict NOx and NH3 emissions, even under ammonia injection fault conditions. The emissions estimated by the EKF observer were compared to those expected if the ATS was working properly, and through a two-dimensional statistical model, it was possible to determine the level of failure in the ammonia injection and correct it for standard operating levels.

The content of the article is organized as follows. The experimental apparatus and the performed tests are presented in Section 2, "Experimental set-up". Followed by Section 3, 'Methodology', which presents the problem addressed, the feasibility of detecting the ammonia injection failure through emissions using model-based fault diagnosis, as well as the statistical methods used and the proposed methodology. The discussion of the results is presented in Section 4. Lastly, in Section 5, the conclusions can be found.

2. Experimental set-up

For the development of this work, the engine used was a Euro 6c turbocharged four-cylinder light-duty engine, with high-pressure exhaust gas recirculation (HP-EGR), a variable geometry turbine (VGT), and a common rail direct injection system. Additional engine information is shown in Table 1.

Table 1
Engine characteristics.

Displaced volume	1499 cm^3
Bore × Stroke	75 × 84.8 mm
Compression ratio	16.4:1
Maximum torque	300 N m @ 1750 rpm
Maximum power	96 kW @ 3750 rpm
Emissions standard	Euro 6c

Table 2
SCRF catalyst parameters.

Diameter × length	0.07 × 0.3 m
Cell density	600 cpsi
Wall thickness	0.8 mm
SCR storage capacity	80 mol/m^3
Surface coverage	0.037431 [–]
Critical surface coverage	0.1995 [–]

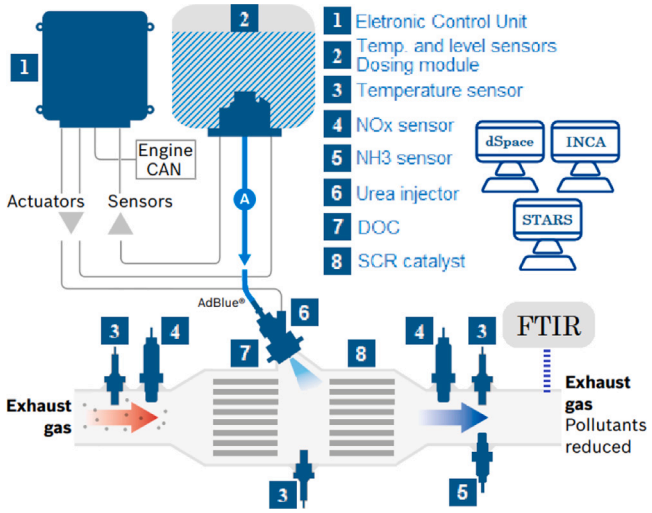

Fig. 2. After-treatment system set-up.

The engine was coupled to a Horiba DYNAS3 asynchronous dynamometer and controlled by Horiba's integrated STARS automation system, where system settings and monitoring were accessed. Through the road load simulation (RLS) module, it was possible to implement and perform the driving cycles used to develop this work.

As the ammonia injection needed to be controlled according to the proposed strategy, created a bypass signal in the INTECRIO platform and built-in the dSpace MicroAutobox system, connected via an ETK-ECU interface, the ECU calibration was done through the INCA platform. The main configuration consisted of a Microautobox II real-time system, ETAS ES910 prototyping and interface module, and an open electronic control unit (ECU).

Regarding the ATS, which consists of a system that integrates SCR with a particle filter (SCRF), Table 2 presents additional catalyst information.

In addition, several sensors were placed in the exhaust line, such as NOx, NH3 and temperature sensors. As well as a Fourier Transform Infrared Spectroscopy (FTIR) gas analyser to compare with the sensors' measurement. Horiba fuel flow meter and others conventional sensors (mass airflow, boost pressure, etc.) are also part of the experimental set-up.

The complete experimental set-up can be seen in Fig. 2, as well as a more detailed description of the emission and temperature equipment are shown in Table 3.

Regarding the tests performed, three sets of tests were used. First, tests were carried out with constant failure in the ammonia injection. Different Worldwide harmonized Light vehicles Test Cycle (WLTC) cycles were performed with 3 levels of injection factor (I.F.), 25%, 50% and 75% of the standard injection, which are, respectively, I.F. = 0.25, 0.50 and 0.75, and with the standard injection (I.F. = 1.00), these injection failures are artificially produced, bypassing the nominal value of the ammonia injection multiplied by the I.F., thus changing the injector opening time. Note that, for I.F. = 0.75, the amount of ammonia injected is approximately 75% of what is required. However, the signal feedback to the ECU is the integral value of the injection. The same strategy has been used to simulate other failure levels. Thus, the I.F. refers to the level of the ammonia failure invisible to the control strategy.

Table 3
Equipment specifications.

Equipment	Measurement
FTIR	NOx 0–2000 ppm ±1.0% of full scale NH3 0–1100 ppm ±1.0% of full scale
NOx sensor	0–1860 ppm ±15 ppm @0–1000 ppm ±1.5% @≤1000 ppm
NH3 sensor	0–1500 ppm ±1.5% of full scale
Thermocouple	−270–1260 °C ±2.2% °C - Type K

Secondly, several WLTC cycles with different I.F. were carried out in sequence, to validate the proposed methodology.

Finally, a set of tests were performed in a merged cycle, WLTC plus Standardized Random Test (RTS), as seen in Fig. 3, and without correction of the injection failure. In cases where injection failure is considered, a constant degradation rate was applied to check the capability of the proposed strategy of tracking the injection fault and applying the proper correction.

3. Methodology

3.1. Proposed strategy approach

The proposed strategy is based on the simple observation that if there is any failure in ammonia injection, this event must have an impact on the exhaust emissions [19].

As can be seen in Fig. 4, with the increase of the error in the ammonia injection, the NH3 slip is reduced since all the ammonia injected is absorbed and used in the reduction reaction with NOx entering the catalyst (upper plot). Otherwise, NOx slip remains constant for errors below 50% (I.F. = [0.5; 0.75; 1.00]) of the nominal injection (bottom plot). This is related to two main facts: first, due to the strong NOx restrictions, the SCR catalyst is forced to work with high NOx conversion rates, which usually leads to some level of NH3 slip [20]. To deal with the NH3 slip appearing, even when the system works in design conditions, engines are usually equipped with an Ammonia Slip Catalyst (ASC) [21]. Second, to reduce NOx, the ammonia injected must be previously absorbed and stored by the catalyst, so the SCR is a dynamic system with complex relations between ammonia injection and emissions that makes difficult its control without any slip in changing conditions such as the WLTC [22].

These concepts are important, since the strategy to detect the level of ammonia injection failure is based on the comparison of NOx and NH3 accumulated over a predetermined period, between cycles with and without ammonia injection failure. Thus, allowing access and quantifying errors between these situations.

Once it was checked that the failure in the ammonia injection could be observed through the exhaust emissions, the following steps were taken in order to verify the viability of the proposed strategy.

- During the engine operation, the NOx emissions before the SCR are accumulated until reaching a calibrated value. The time needed to reach these NOx emissions will define a window where the analysis will be done. Contrary to the strategy adopted by

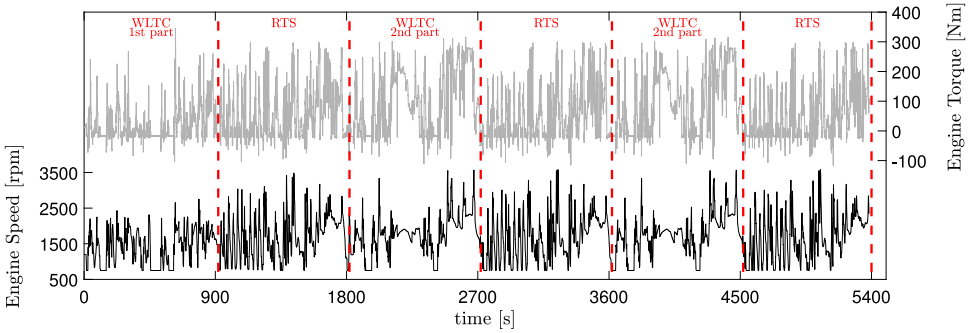

Fig. 3. Merged driving cycle WLTC+RTS. Cycle used to validate the proposed methodology.

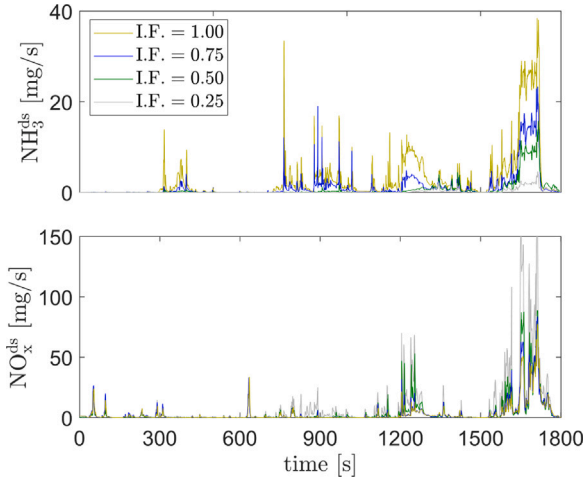

Fig. 4. Slip of NH3 (upper plot) and NOx (bottom plot) for different levels of ammonia injection failure.

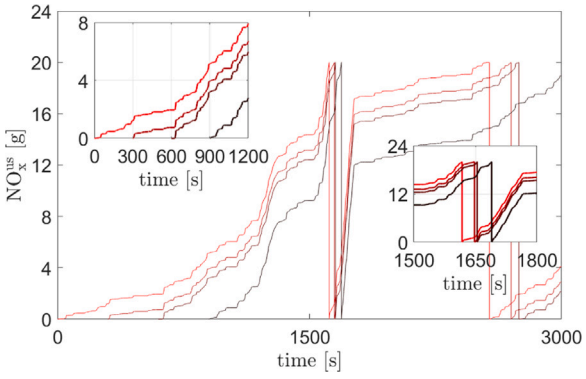

Fig. 5. Different starting points for the accumulation window of NOx upstream of the SCR catalyst.

Mora et al. [15], instead of accumulating in a fixed time-window, NOx emissions before the catalyst are used as a reference, then the considered window is adapted to the operating conditions. The NOx threshold should be calibrated to allow injection fault detection, considering aspects such as the impact of injection fault on NOx reduction efficiency, modelling, and sensor errors. The accumulation windows size number i of a given test (AWS_i) will be determined by the time needed by the NOx emissions upstream the SCR to reach a given mass according to the following expression (Eq. (1)):

$$\sum_{n=1}^{AWS_i} NO_{x,n}^{us}\delta t = NO_x^{up,thr}, \quad (1)$$

where, NO_x^{us} [mg/s] is the NOx mass flow before the catalyst, which is integrated from the start of the window i (n=1) until the threshold value ($NO_x^{up,thr}$) is reached to define the window size AWS_i.

A new window is started once a window finishes or after a calibrated time, in the case at hand 300 s, so depending on the conditions, several windows can be run in parallel, with a maximum of 4 for the current work. Fig. 5 shows an example for two consecutive WLTCs with $NO_x^{up,thr}$ = 20 g. Note that despite the first two windows starting with 300 s difference, they both finish around second 1600 s due to the increase in NOx emissions as the driving cycle evolves.

- The AWS found in the previous step is used to integrate the NOx (Eq. (2)) and NH3 (Eq. (3)) emissions downstream the SCR.

$$\text{Accumulated } NO_{x,i}^{ds} = \sum_{n=1}^{AWS_i} NO_{x,n}^{ds}\delta t, \quad (2)$$

$$\text{Accumulated } NH_{3,i}^{ds} = \sum_{n=1}^{AWS_i} NH_{3,n}^{ds}\delta t, \quad (3)$$

Fig. 6 shows the evolution of the NOx upstream and downstream SCR (top and middle plots) and NH3 downstream the SCR (bottom plots) with the corresponding accumulated values for the first window. Note how downstream emissions are integrated during the window and that when the integral of the NOx upstream reaches the threshold (in the case at hand 20 g), the window is restarted.

- The previous process is performed for 3 different levels of ammonia injection failure, 25 (I.F. = 0.25), 50 (I.F. = 0.50) and 75 (I.F. = 0.75) percent of the nominal injection, and the nominal injection (I.F. = 1.00). In this way, it is possible to create a distribution of the NOx and NH3 accumulated emissions in the considered windows for every injection failure.
- The same steps are performed for different values of the threshold for NOx emissions upstream SCR ($NO_x^{up,thr}$), in order to calibrate the value that allows the separation between the distributions for the different injection faults. Fig. 7 lower plot shows the locations in the NOx-NH3 downstream SCR plane of the results obtained with different NOx upstream thresholds. Upper plots show the fit to a normal distribution of the results. Note that a larger accumulation window is required for distributions to be more separate, consequently requiring a longer time to detect the injection failure.

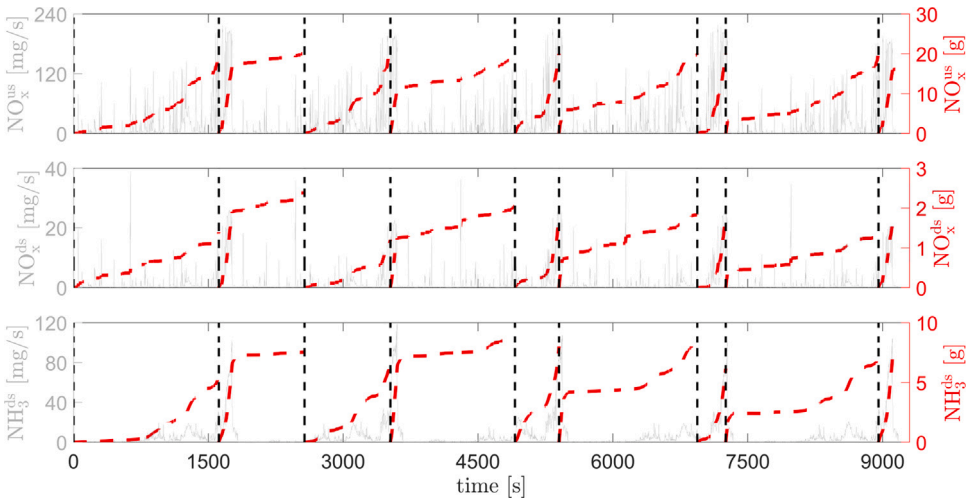

Fig. 6. Emissions evolution of 5 consecutive WLTC cycles. Upper plot: SCR NOx upstream responsible for the definition of the AWS, the windows have different accumulation times, but the same amount of total NOx (20 g). Middle and bottom plot: signals used to calibrate the NOx and NH3 distribution.

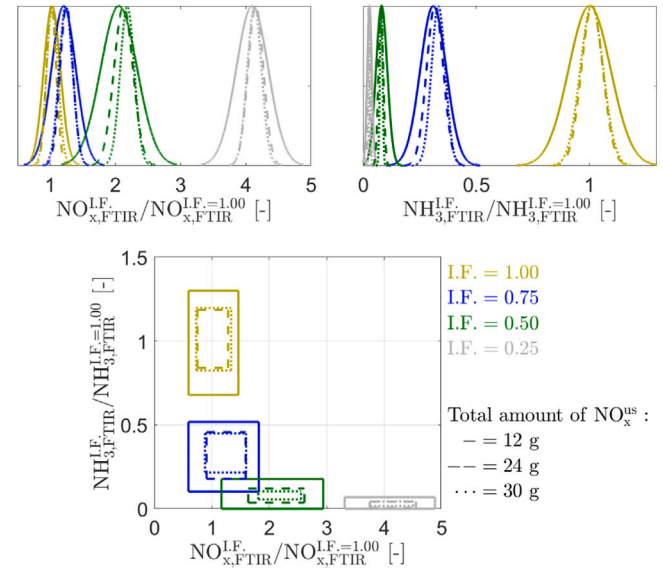

Fig. 7. Normal distribution of NOx and NH3 slip for different levels of ammonia injection failure and different accumulation windows size (12, 24 and 30 g - upper plots) using the FTIR emissions signal. (For interpretation of the references to colour in this figure legend, the reader is referred to the web version of this article.)

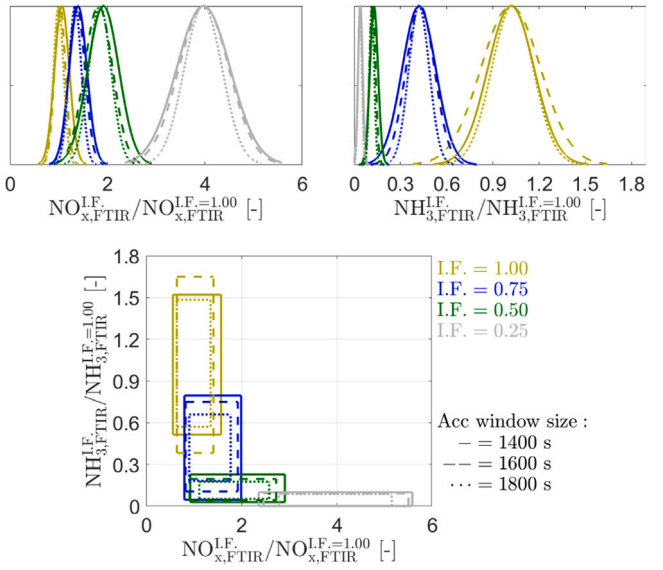

Fig. 8. Normal distribution of NOx and NH3 slip for different levels of ammonia injection failure and different accumulation windows size (1400, 1600 and 1800 s - upper plots) using the FTIR emissions signal.

With the distribution, it was possible to verify that, in terms of NH3, errors higher than 50% of the nominal injection are indistinguishable (grey and green distributions). With higher injection faults than 50%, the amount of ammonia available is so low that all the injected ammonia reacts with the NOx entering the catalyst, being the NH3 slip very small.

Regarding NOx, it is not possible to differentiate the nominal injection from errors lower than 25% (yellow and blue distributions). Even for this level of error the catalyst operates with high efficiency rates.

The proposed methodology was also compared when it uses a fixed time window to reset the accumulation window, instead of SCR NOx upstream, as proposed by Mora et al. [15], the distribution results can be seen in Fig. 8.

Using a fixed time window, it was not possible to separate the error levels in the ammonia injection failure. The use of a fixed time window has several drawbacks, as also commented by Wang et al. [18], mainly because depending on where the time window starts, there will be a big difference in the accumulated values of NOx and NH3 downstream of the catalyst, this difference makes the distribution very broad, since the use of AWS fixed does not create any linkage of pollutants to a physical parameter. The comparison of duration and number of windows between fixed and variable AWS as can be seen in Fig. 9.

As the cycle evolves, the AWS duration decreases as the cycle goes from the low load zone towards the high/very high load zone and starts to grow when AWS starts the next cycle (the evolution of the cycles is presented in Fig. 6). This approach allows the use of variable time windows, but constant in NOx at the catalyst inlet, consequently in areas where NOx production is low, there is more time for data collection, allowing enough information to detect the level ammonia injection failure.

3.2. Observer and model design

The proposed strategy for ammonia injection failure is based on the comparison of the observed versus the expected emissions in a given

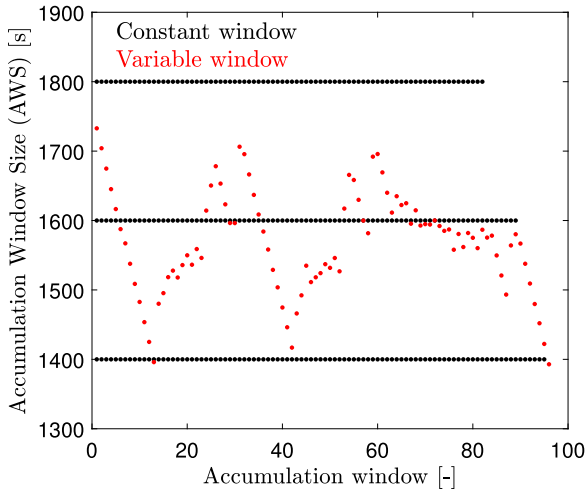

Fig. 9. Comparison of duration and number of windows for fixed and variable accumulation window size. Dark dots: fixed AWS. Red dots: variable AWS (proposed approach). (For interpretation of the references to colour in this figure legend, the reader is referred to the web version of this article.)

time window. One may think that if a model with a suitable accuracy is calibrated to represent emissions of the system without failure and an observer of the actual NOx and NH3 emissions are available, the system can be diagnosed from the deviations between the observed and modelled values without fault.

From these assumptions, models for NOx and NH3 emissions have been developed based on the following hypothesis:

(i) In order to maximize the NOx conversion efficiency, current strategies keep the ammonia coverage ratio of the catalyst (i.e., the ratio of the amount of ammonia absorbed by the catalyst to the maximum absorption capacity [23]) at the highest possible level without excessive NH3 slip [24]. Therefore, NOx dynamics after the catalyst is mainly dependent on NOx dynamics before catalyst, since the SCR is always working with high NOx conversion efficiency rates [25].

(ii) The NH3 emissions dynamics are considerably slower than NOx [25,26]. Since the ammonia coverage varies slowly, the NH3 slip that depends on it will also vary slowly.

(iii) NOx sensors working properly, being the only deviation between the actual and measured NOx value due to the impact of cross-sensitivity to ammonia on the sensor reading.

3.3. Artificial neural network model

The assumptions (i) and (ii) allow to model the catalyst as a dynamic input–output system, since it is possible to represent the behaviour of the system through the relation of the input and output data [27]. Due to hypothesis (i), i.e., the NOx dynamics after the SCR are dominated by the NOx signal upstream the SCR, a two-layer feed-forward artificial neural network (ANN) was developed to model NOx. The ANN has four input and one output signal, with one hidden and one output layer. A set of twenty different tests were used to develop the ANN, covering engine maps, steady-state conditions and driving cycles. The ANN was developed as follows:

- Data assembly definition. NOx upstream of the SCR (NO_x^{us} [ppm]), ammonia injected (NH_3^{inj} [mg/s]), exhaust gas mass flow (m_{exh} [kg/h]) and SCR catalyst temperature (T_{SCR} [°C]) were set as inputs, whilst NOx slip ($NO_{x,ANN}$ [mg/s]) as output.
- ANN structure. The hidden layer of ANN has ten hidden neurons and uses a sigmoid transfer function, while the output layer has one neuron and linear transfer function.
- ANN training and validation. The ANN algorithm training uses the Levenberg–Marquardt back-propagation approach (least squares analysis widely used to train and solve feed-forward ANN [28]). The training process recursively adjusts the bias and weight of the ANN to minimize a given function to its local minimum. For all training input and output variables, the error was calculated as:

$$J(b,w) = \frac{1}{2}\sum_{n=1}^{N}\sum_{m=1}^{M}(y_{n,m} - \hat{y}_{n,m})^2, \tag{4}$$

where b is the bias and w the weight vector; N the inputs; M the outputs; y the target vector and ŷ the output vector.

The dataset used in each stage of the ANN development can be seen in Fig. 10.

Through the ANN output (NOx slip), it is possible to estimate the NH3 slip using the NOx sensor signal downstream SCR [29],

$$NH_3 = \frac{NO_{x,sensor} - NO_x}{K_{CS}}, \tag{5}$$

where $NO_{x,sensor}$ [ppm] is the NOx sensor signal concentration, NO_x [ppm] and NH_3 [ppm] are the actual NOx and NH3 concentrations measured by FTIR, and K_{CS} [−] is the cross-sensitivity factor, which can be modelled as a factor dependent on the NH3 concentration. To estimate the K_{CS}, a simple model developed by Pla et al. [30] was used:

$$K_{CS} = 1.1286 - 0.5992\ \exp(-8.4237 \times NH_3), \tag{6}$$

Note that there is an algebraic loop between Eqs. (5) and (6), as K_{CS} is needed to calculate NH_3 and vice versa. Considering the slow variation in K_{CS} and NH_3, a sample delay (0.1 s) in K_{CS} was used.

3.4. Sensors signal analysis model

The sensor signal analysis (SSA) model exclusively uses information from the NOx sensor placed upstream and downstream of the SCR catalyst, although the downstream signal is affected by cross-sensitivity, the model is able to minimize this impact. In addition, unlike ANN, the model does not depend on the ammonia injection feedback. Therefore, any error in the signal does not affect the model's prediction.

The SSA model considering the assumptions (i) and (ii) was developed as follows:

The NOx sensor signals upstream ($NO_{x,sensor}^{us}$ [ppm]) and downstream ($NO_{x,sensor}^{ds}$ [ppm]) of the catalyst is stored in a calibrated buffer, and their average values are used to estimate the average NOx conversion efficiency ($\overline{\eta_{NO_x}}$) in the considered time-window, and is calculated as follows:

$$\overline{\eta_{NO_x}} = 1 - \frac{\overline{NO_{x,sensor}^{ds}} - \overline{K_{CS}} \times \overline{NH_3}}{\overline{NO_{x,sensor}^{us}}}, \tag{7}$$

where $\overline{NH_3}$ and $\overline{K_{CS}}$ represent the average values during the time-window, calculated from Eqs. (5) and (6), respectively. Considering hypothesis (i), it is feasible to assume that instantaneous and average NOx conversion efficiency are equal during the time window $\eta_{NO_x} = \overline{\eta_{NO_x}}$.

Applying the conversion efficiency calculated by Eq. (7) it is possible to estimate the NOx slip as:

$$NO_x = NO_{x,sensor}^{us}(1 - \eta_{NO_x}), \tag{8}$$

The NH3 slip can be computed via Eq. (5) considering an average K_{CS} and an average NOx slip from Eq. (8),

$$\overline{NH_3} = \frac{\overline{NO_{x,sensor}^{ds}} - \overline{NO_x}}{\overline{K_{CS}}}, \tag{9}$$

$\overline{NH_3}$ and $\overline{NO_x}$ are the average emissions during the time-window. Since the dynamics of the NH3 slip varies slowly, a proper calibration of the

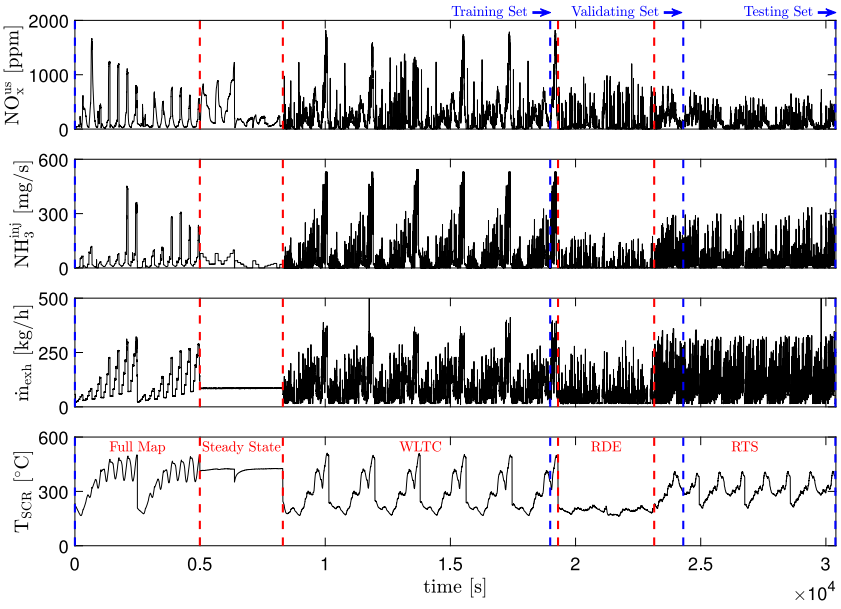

Fig. 10. Evolution of the signals that feed the development of the neural network in its different stages.

buffer size allows to estimate the NH3 slip accurately, in the present case, a buffer of 200 samples at 10 Hz was used. In this sense and according to hypothesis (ii), it is assumed that: $NH_3 = \overline{NH_3}$.

3.5. Extended Kalman filter applied to the models

Considering a generic dynamic system applied to an observer structure,

$$x_k = f(x_{k-1}, u_{k-1}) + w_k, \tag{10a}$$

$$y_k = h(x_k) + v_k, \tag{10b}$$

where x_k represents the state estimation of the model, u_k and y_k are the measurements of inputs and outputs, respectively. w_k is the process noise, and v_k the observation noise. The complexity of the functions f and h determine the model accuracy. However, any model has some level of uncertainty. In order to increase accuracy and robustness, Eq. (10) can be represented in observer form:

$$\hat{x}_k = f(\hat{x}_{k-1}, u_{k-1}) + K(y_k - \hat{y}_k), \tag{11a}$$

$$\hat{y}_k = h(\hat{x}_k), \tag{11b}$$

where $\hat{y}_k$ is the output of the observed state estimation $\hat{x}_k$, u_k is the measurement of the inputs and K is the Near-optimal Kalman gain. Where the state of the system is continuously updated by the observer through new measurements ($K(y_k - \hat{y}_k)$).

The EKF algorithm consists of two main events: Predict and Update. The prediction phase uses the state and covariance estimate in the previous step to obtain an estimate of the current state, and in the update phase, the prediction is combined with the current observation to refine the state and covariance estimate [31,32].

At each iteration, the EKF algorithm proceeds as follows:

- Prediction step:
  - Predict state estimate: $\hat{x}_{k|k-1} = f(\hat{x}_{k-1}, u_k)$ The model is applied to the previous state observation ($\hat{x}_{k-1}$) with current inputs (u_k) leading to first state estimation.
  - Predict covariance estimate: $P_{k|k-1} = F_k P_{k-1} F_k^T + Q_k$ An initial observer covariance estimation is calculated from the previous value of the covariance (P_{k-1}), the process covariance (Q_k) and the Jacobian of the state F_k defined as: $F_k = \left|\frac{\partial f}{\partial x}\right|_{\hat{x}_{k-1}, u_k}$
- Update step
  - Measurement residual: $\hat{e}_k = y_k - \hat{y}_k = y_k - h(\hat{x}_{k|k-1})$ Compute the difference between the sensor reading (y_k) and the observer estimation of the sensor reading ($\hat{y}_k = h(\hat{x}_{k|k-1})$).
  - Residual covariance: $S_k = H_k P_{k|k-1} H_k^T + R_k$ The covariance residual is calculated from the state covariance prediction ($P_{k|k-1}$), the measurement covariance (R_k) and the Jacobian of the model output function (H_k) defined as: $H_k = \left|\frac{\partial h}{\partial x}\right|_{\hat{x}_{k|k-1}}$
  - Kalman gain: The gain (K) is directly proportional to the covariance prediction and inversely proportional to the residual one $K_k = \frac{P_{k|k-1} H_k^T}{S_k}$
  - Update state estimate: $\hat{x}_k = \hat{x}_{k|k-1} + K_k \hat{e}_k$ The observer state update is calculated from the predicted state, and the measurement residual weighted with the Kalman gain.
  - Update covariance estimate: $P_k = (I - K_k H_k) P_{k|k-1}$

Regarding the dynamic system, it is composed of two states, $x_1 = \zeta_{NO_x}$ and $x_2 = NH_3$, where ζ_{NO_x} is the NOx bias and NH_3 is the NH3 concentration downstream of the SCR. Two inputs $u_1 = NO_{x,sensor}$ and $u_2 = NO_{x,ANN}$ obtained from NOx sensor and ANN model, respectively, and one output measurement (y), whose behaviour is governed by the following equations:

$$x_k = f(x_{k-1}, u_{k-1}) = \begin{cases} x_{1,k} = x_{1,k-1} + w_{1,k} \\ x_{2,k} = \frac{u_{1,k-1} - (u_{2,k-1} + x_{1,k-1})}{K_{CS}(x_{2,k-1})} + w_{2,k} \end{cases} \tag{12}$$

$$y_k = h(x_k) = x_{2,k} + v_k \tag{13}$$

where w_1 and w_2 are the noises associated to the states. Note that, in the first state (x_1), the bias in the NOx estimate is assumed not to change abruptly and the changes are only associated with noise, the second state (x_2) is calculated according to Eq. (5), and NH3 slip of the SSA model is considered as a measurement (y).

For the system to be considered observable, the observability matrix and the number of states of the system must be equal. [33], where the observability matrix is defined by:

$$\Omega = \begin{bmatrix} \frac{\partial h}{\partial x} \\ \left[\frac{\partial h}{\partial x}\right]\left[\frac{\partial f}{\partial x}\right] \end{bmatrix} \tag{14}$$

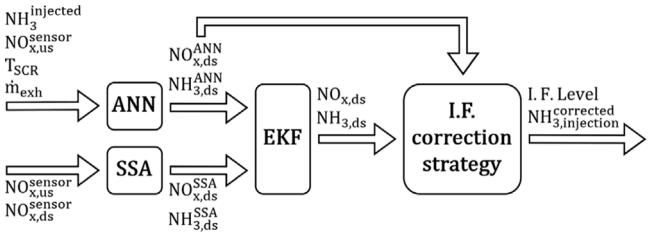

Fig. 11. Flowchart of inputs and outputs of control-oriented models, EKF and ammonia injection correction strategy.

From the dynamic system Eqs. (12) and (13):

$$\frac{\partial h}{\partial x} = [0\ 1] \tag{15a}$$

$$\frac{\partial f}{\partial x} = \begin{bmatrix} 1 & 0 \\ -\frac{1}{K_{CS}(x_{2,k-1})} & -\frac{\frac{\partial K_{CS}}{\partial x_2}(u_{1,k}-(u_{2,k}+x_{1,k-1}))}{K_{CS}(x_{2,k-1})^2} \end{bmatrix} \tag{15b}$$

Therefore, the observability matrix becomes:

$$\Omega = \begin{bmatrix} 0 & 1 \\ -\frac{1}{K_{CS}(x_{2,k-1})} & -\frac{\frac{\partial K_{CS}}{\partial x_2}(u_{1,k}-(u_{2,k}+x_{1,k-1}))}{K_{CS}(x_{2,k-1})^2} \end{bmatrix} \tag{16}$$

The system is observable, since the rank of Ω is 2 and the system has 2 states. Therefore, the EKF approach can be applied to ANN and SSA models.

The complete structure of inputs and outputs of the models, EKF and the proposed ammonia injection correction strategy can be seen in the following flowchart (Fig. 11).

3.6. Fault detection strategy extended to observer and models

The method proposed essentially extends the analysis of the emissions sensitivity to injection faults represented by Fig. 7 to be applied online. To this aim, the ANN model is assumed to be representative of the emissions without injection failure (I.F. = 1), while the observer is assumed to represent the actual emissions. In this sense, the ratio between the observed and modelled emissions is an estimation of the ratio between the emissions with a given injection fault (I.F. < 1) and without fault (I.F. = 1).

The same procedure presented in Section 3.1 is applied to the models to create a probability distribution.

Note that, in this case (Fig. 12), the distribution is not directly the normalized value itself, but the relation between the model's behaviour and the observer. This relation can be used, since ANN depends on the feedback signal from the ammonia injector, its error in estimating emissions tends to increase as the ammonia injector failure also increases.

With this distribution, it is possible to verify that, in terms of NOx, with increased injection failure, less ammonia is injected and, consequently, there is a lower conversion rate of NOx. Since the actual NOx emissions are higher than those estimated by ANN that would be representative of the system without injection fault, the probability distribution tends to values greater than one. The opposite is true for NH3 emissions, since the real NH3 slip is lower than estimated by the ANN, the probability distribution tends to be lower than one.

It is worth mentioning that the accuracy of the diagnosis will depend on the correct calibration of the upstream NOx SCR threshold (Eq. (1)) and on the accuracy of the models themselves to estimate NOx and NH3 emissions, being these estimates impacted by the intrinsic error of the computational models, but also after a long period of time by the catalyst ageing.

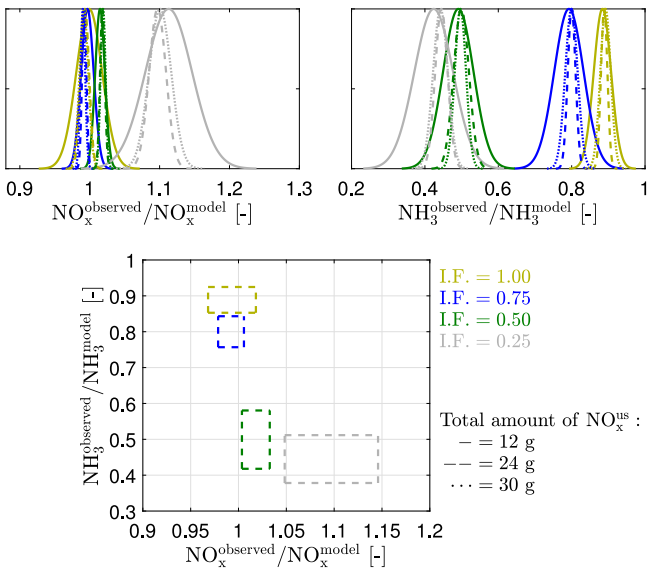

Fig. 12. Normal distribution of NOx and NH3 slip for different levels of ammonia injection failure and different accumulation windows size (12, 24 and 30 g - upper plots) using the model/observer ratio emissions signal.

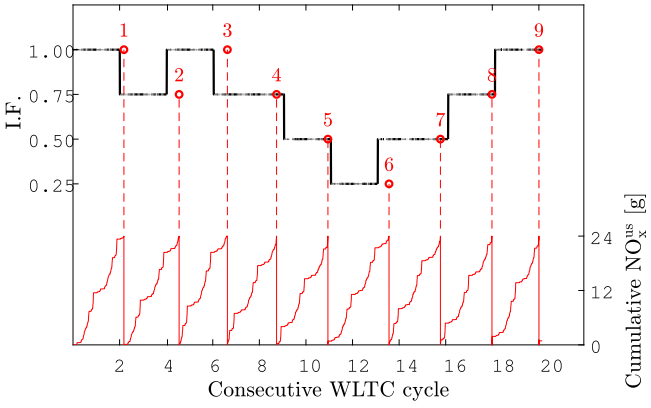

Fig. 13. Actual level of the ammonia injection failure and estimate at the end of the accumulation window for 20 consecutive WLTC cycles.

4. Results and discussion

4.1. Real-time strategy application for constant failure in ammonia injection

In order to assess the capacity of the proposed strategy to track the level of the ammonia injection failure, the model was tested in 20 WLTC cycles in sequence, with different fault levels. In Fig. 13, the upper part, the dark dashed line is the current level of the ammonia injection failure, and the red circles, the model estimation for the failure level at the end of the AWS.

As can be seen in Fig. 13, at the end of each accumulation window, the model was able to estimate the level of error that the system was subjected to during the previous period. In the current case, to accumulate 24 g of NOx before the SCR catalyst, more than one complete WLTC cycle is needed, for this reason, the estimated failure level (red circles) represents the current failure level to which the system is mostly subjected during the accumulation window.

In Fig. 14, it is possible to verify where each estimated point was placed in the normal distribution graph. As can be seen, not all the points were within the range of distributions, but classifying the points

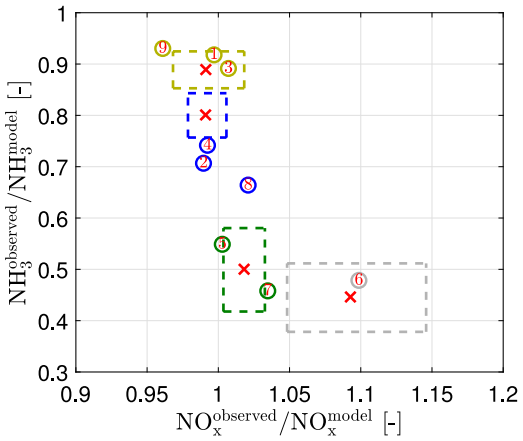

Fig. 14. Estimated results of the ammonia injection failure level in the normal distribution graph of NOx and NH3 slip in a 24 g accumulation window.

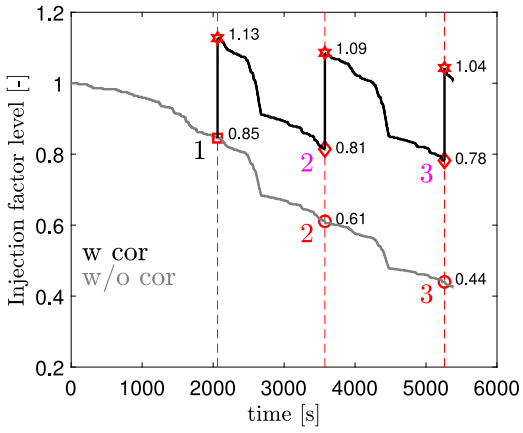

Fig. 15. Injection factor level during a WLTC+RTS merged cycle and degradation of the ammonia injection system, with (dark line) and without (grey line) ammonia injection correction. (For interpretation of the references to colour in this figure legend, the reader is referred to the web version of this article.)

as their closest clusters provides accurate results (red x).

$$\text{I.F.} = \underset{j}{\text{argmin}} \sqrt{\left(\frac{NO_x^{obs}}{NO_x^{model}} - C_j^{NO_x}\right)^2 + \left(\frac{NH_3^{obs}}{NH_3^{model}} - C_j^{NH_3}\right)^2}, \quad (17)$$

where, $j = [0.25, 0.50, 0.75, 1.00]$ and C it is the centroid of each distribution.

4.2. Real-time strategy application for ammonia injection system degradation

The correction application in the degradation of the ammonia injection system was carried out in two steps: first, a merged cycle (WLTC and RTS) was performed, where no correction was made in the ammonia injection, this test was performed to validate the capacity of the proposed methodology in detecting the degradation of the ammonia injection system. In the second step, the same cycle was carried out, and the correction was applied to the ammonia injection from the error level detected. It consists of increasing the demand of ammonia to compensate the injection error. This test was performed to assess the methodology's capacity to correct the injection failure.

Since the strategy is aimed to correct the ammonia injection, failure levels greater than 50% of the nominal injection (I.F. = 0.50) are not expected. Therefore, the NOx distribution is unnecessary, as it only distinguishes I.F. = 0.25 from I.F. = 0.50, as shown in Fig. 12.

In Fig. 15, it is possible to see the ratio between the applied ammonia injection and the reference injection without failure for both cases: without correction (grey) and with the proposed correction (black). As the cycle evolves, injector degradation makes the injector factor decrease, while corrections lead to an increase in the injector factor after the fault diagnosis. The red markers refer to the points at the end of the accumulation window, being the circles and the stars, without and with correction of the ammonia injection, respectively.

At the end of each accumulation window, the proposed strategy was able to detect and correct the level of ammonia injection, at the same time reducing the impact of system degradation. Of course, the correction is not able to keep the I.F. = 1 since, it requires some time (where degradation is evolving) for diagnosis, and both the model and observer have some error.

Fig. 16 shows where each estimated point was placed at the end of each accumulation window in the NH3 distribution. As can be seen, for ammonia injection without correction, point 3 (the end of the complete cycle) has an error level of 50% of the nominal injection (I.F. = 0.50), while with the correction the error level remains 25% (I.F. = 0.75).

As final results, Figs. 17 to 19 show the NOx and NH3 emissions and also the ammonia injection. Dark lines refer to signals with correction

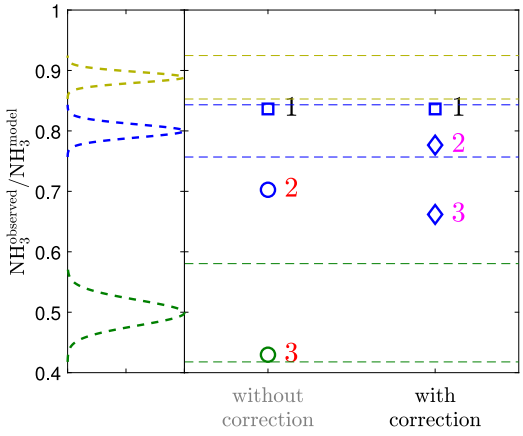

Fig. 16. Estimated results of the level of failure in ammonia injection in terms of NH3 slip.

in ammonia injection, grey lines to signals without correction, both for tests with constant degradation of ammonia injection, and red lines to signals when there is no degradation of the ammonia injection system.

Fig. 17 shows the NOx slip emissions, as can be seen, when the ammonia injection is corrected it tends to similar levels as when there is no injection failure, being slightly higher (5.35%). However, when compared to degradation of the ammonia injection system without correction, NOx emissions rise by 23.33%.

It is possible to verify that up to approximately 2700 s the NOx conversion level remains similar for all cases, even in the case of the injection system degradation without correction is about 70%, this is in line with the previous discussion (Fig. 4), for injection failure levels around 75% the SCR catalyst is still capable of converting NOx with high efficiency, since the NOx conversion occurs by the amount of ammonia previously stored [23].

In terms of NH3 slip, as can be seen in Fig. 18, there is an increase in NH3 emissions for both cases, being 18.67% and 46.41% for tests with and without correction in the ammonia injection, respectively. This behaviour was already expected for two main reasons, firstly, current ammonia injection strategies aim to reduce NOx emissions as much as possible, being on the limit between storing the maximum amount of ammonia inside the catalyst without starting the slip. Second, the estimation of the catalyst load is performed through models, and estimating it accurately is a difficult task when applied to dynamic systems, consequently leading to unwanted NH3 slip.

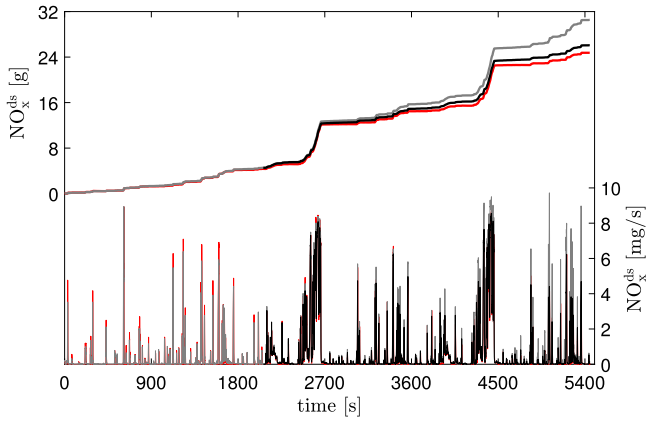

Fig. 17. NOx slip with (dark line) and without (grey line) ammonia injection correction and NOx slip without ammonia injection failure (red line) during a WLTC+RTS merged cycle. (For interpretation of the references to colour in this figure legend, the reader is referred to the web version of this article.)

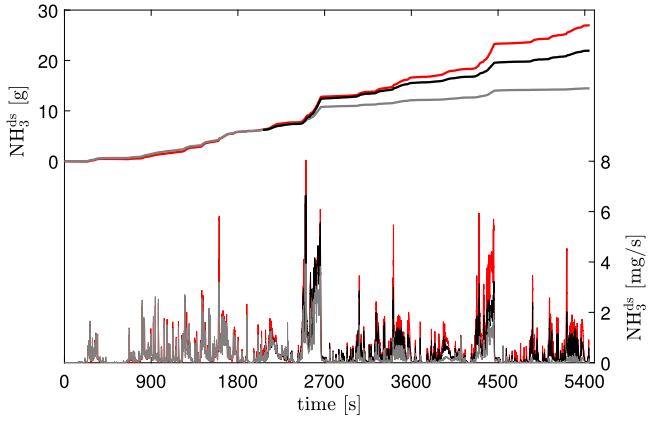

Fig. 18. NH3 slip with (dark line) and without (grey line) ammonia injection correction and NH3 slip without ammonia injection failure (red line) during a WLTC+RTS merged cycle. (For interpretation of the references to colour in this figure legend, the reader is referred to the web version of this article.)

Regarding the total amount of ammonia injected during the cycle, the correction of ammonia injection reaches a similar level to the standard injection strategy, being slightly smaller (5.65%), and as expected, the level of ammonia injected when there is a degradation of the injection system without correction is considerably lower (27.83%).

5. Conclusions

This article explored a novel methodology to detect the failure level in the degradation of an ammonia injection system, as well as to correct it. Through a strategy that uses computational models and statistical methods of normal distribution for different levels of failure in ammonia injection, it was possible to verify that the proposed strategy is capable to estimate and satisfactorily correct such errors. In this way, the proposed methodology can be used in real-time applications for control and diagnostic strategies. The main specific contributions of this work are as follows:

- The proposed model was able to detect and correct ammonia injection in all failure situations. Both in cases with constant failure in standard driving cycles, as well as in a degradation of the injection system in a merged cycle (WTLC+RTS).
- With the ammonia injection correction strategy in cases of failure in the ammonia injection system, it was possible to reduce NOx emissions by 23.33% in a merged cycle. Achieving almost the same level as the standard strategy where there is no failure in the ammonia injection system.
- The proposed methodology, through the use of a variable time window linked to a constant NOx threshold at the SCR input, can be applied to the most diverse cycles and engine operating conditions.

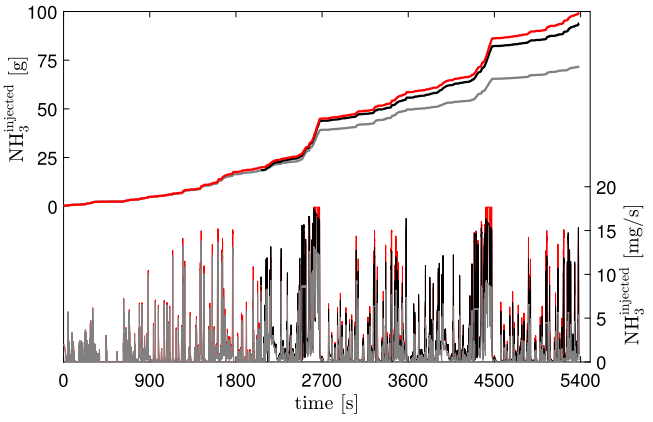

Fig. 19. Ammonia injection with (dark line) and without (grey line) correction and ammonia injection without failure (red line) during a WLTC+RTS merged cycle. (For interpretation of the references to colour in this figure legend, the reader is referred to the web version of this article.)

CRediT authorship contribution statement

Benjamín Pla: Conceptualization, Methodology, Validation, Formal analysis, Investigation, Resources, Writing – original draft, Writing – review & editing, Supervision, Project administration, Funding acquisition. **Pau Bares:** Formal analysis, Supervision, Writing – review & editing. **Enrique José Sanchis:** Formal analysis, Resources, Writing – review & editing, Funding acquisition. **André Nakaema Aronis:** Conceptualization, Methodology, Software, Validation, Formal analysis, Investigation, Writing – original draft, Writing – review & editing.

Declaration of competing interest

The authors declare that they have no known competing financial interests or personal relationships that could have appeared to influence the work reported in this paper.

Acknowledgement

This research has been supported by Grant PID2020-114289RB-I00 funded by MCIN/AEI/10.13039/501100011033.

References

[1] Reitz RD, Ogawa H, Payri R, Fansler T, Kokjohn S, Moriyoshi Y, Agarwal A, Arcoumanis D, Assanis D, Bae C, Boulouchos K, Canakci M, Curran S, Denbratt I, Gavaises M, Guenthner M, Hasse C, Huang Z, Ishiyama T, Johansson B, Johnson T, Kalghatgi G, Koike M, Kong S, Leipertz A, Miles P, Novella R, Onorati A, Richter M, Shuai S, Siebers D, Su W, Trujillo M, Uchida N, Vaglieco BM, Wagner R, Zhao H. IJER editorial: The future of the internal combustion engine. Int J Engine Res 2020;21(1):3–10. http://dx.doi.org/10.1177/1468087419877990.

[2] Margaryan S. Low emission zones and population health. J Health Econ 2021;76. http://dx.doi.org/10.1016/j.jhealeco.2020.102402.

[3] Morfeldt J, Davidsson Kurland S, Johansson DJ. Carbon footprint impacts of banning cars with internal combustion engines. Transp Res D 2021;95. http://dx.doi.org/10.1016/j.trd.2021.102807.

[4] Ni P, Wang X, Li H. A review on regulations, current status, effects and reduction strategies of emissions for marine diesel engines. Fuel 2020;279. http://dx.doi.org/10.1016/j.fuel.2020.118477.

[5] Dey S, Mehta N. Automobile pollution control using catalysis. Resour Environ Sustain 2020;2(November). http://dx.doi.org/10.1016/j.resenv.2020.100006.
[6] Leach F, Kalghatgi G, Stone R, Miles P. The scope for improving the efficiency and environmental impact of internal combustion engines. Transp Eng 2020;1. http://dx.doi.org/10.1016/j.treng.2020.100005.
[7] Namigtle-Jiménez A, Escobar-Jiménez R, Gómez-Aguilar J, García-Beltrán C, Téllez-Anguiano A. Online ANN-based fault diagnosis implementation using an FPGA: Application in the EFI system of a vehicle. ISA Trans 2020;100:358–72. http://dx.doi.org/10.1016/j.isatra.2019.11.003.
[8] Maizak D, Wilberforce T, Olabi A. Denox removal techniques for automotive applications – A review. Environ Adv 2020;2. http://dx.doi.org/10.1016/j.envadv.2020.100021.
[9] Calle-Asensio A, Hernández J, Rodríguez-Fernández J, Lapuerta M, Ramos A, Barba J. Effect of advanced biofuels on WLTC emissions of a euro 6 diesel vehicle with SCR under different climatic conditions. Int J Engine Res 2021. http://dx.doi.org/10.1177/14680874211001256.
[10] Liu Z, Dizqah AM, Herreros JM, Schaub J, Haas O. Simultaneous control of NOx, soot and fuel economy of a diesel engine with dual-loop EGR and VNT using economic MPC. Control Eng Pract 2021;108. http://dx.doi.org/10.1016/j.conengprac.2020.104701.
[11] Li W, Li H, Gu S, Chen T. Control engineering practice process fault diagnosis with model- and knowledge-based approaches : Advances and opportunities. Control Eng Pract 2020;105(February). http://dx.doi.org/10.1016/j.conengprac.2020.104637.
[12] Hu J, Zheng S, Liu X, Wang M, Deng J, Yan F. Optimizing the fault diagnosis and fault-tolerant control of selective catalytic reduction hydrothermal aging using the unscented Kalman filter observer. Fuel 2021;288. http://dx.doi.org/10.1016/j.fuel.2020.119827.
[13] Huang H, Chen Y, Li Z, Wang H, Hao B, Chen Y, Lei H, Guo X. Analysis of deposit formation mechanism and structure optimization in urea-SCR system of diesel engine. Fuel 2020;265. http://dx.doi.org/10.1016/j.fuel.2019.116941.
[14] Vignesh R, Ashok B. Critical interpretative review on current outlook and prospects of selective catalytic reduction system for De-NOx strategy in compression ignition engine. Fuel 2020;276. http://dx.doi.org/10.1016/j.fuel.2020.117996.
[15] Mora J, Willems F, Seykens X, Guardiola C. An OBD strategy to estimate SCR ageing and detect urea injection faults. IFAC-PapersOnLine 2018;51(31):369–76. http://dx.doi.org/10.1016/j.ifacol.2018.10.076.
[16] Canova M, Midlam-Mohler S, Pisu P, Soliman A. Model-based fault detection and isolation for a diesel lean trap aftertreatment system. Control Eng Pract 2010;18(11):1307–17. http://dx.doi.org/10.1016/j.conengprac.2009.10.004.
[17] Arsie I, Cricchio A, De Cesare M, Lazzarini F, Pianese C, Sorrentino M. Neural network models for virtual sensing of NO x emissions in automotive diesel engines with least square-based adaptation. Control Eng Pract 2017;61:11–20. http://dx.doi.org/10.1016/j.conengprac.2017.01.005.
[18] Wang Y-Y, Sun Y, Chang C-F, Hu Y. Model-based fault detection and fault-tolerant control of SCR urea injection systems. IEEE Trans Veh Technol 2016;65(6):4645–54. http://dx.doi.org/10.1109/TVT.2015.2463115.
[19] Hu J, Zeng J, Wei L. Failure diagnosis and tolerant control method for hydrothermally aged SCR system by utilizing EKF observer and MRAC controller. Energy 2018;156:103–21. http://dx.doi.org/10.1016/j.energy.2018.05.094.
[20] Donkers M, Schijndel JV, Heemels W, Willems F. Optimal control for integrated emission management in diesel engines. Control Eng Pract 2017;61:206–16. http://dx.doi.org/10.1016/j.conengprac.2016.03.006.
[21] Colombo M, Nova I, Tronconi E, Schmeißer V, Bandl-Konrad B, Zimmermann L. Experimental and modeling study of a dual-layer (SCR+PGM) NH3 slip monolith catalyst (ASC) for automotive SCR aftertreatment systems. Part 1. Kinetics for the PGM component and analysis of SCR/PGM interactions. Appl Catal B 2013;142–143:861–76. http://dx.doi.org/10.1016/j.apcatb.2012.10.031.
[22] Rajesh Chundru V, Parker GG, Johnson JH. Development of a Kalman filter estimator for simulation and controlof NO x and PM in a SCR catalyston a DPF. Int J Engine Res 2020. http://dx.doi.org/10.1177/1468087420954041.
[23] Pla B, Bares P, Sanchis E, Aronis A. Ammonia injection optimization for selective catalytic reduction aftertreatment systems. Int J Engine Res 2021;22(7):2169–79. http://dx.doi.org/10.1177/1468087420933125.
[24] Yang S, Feng S, Sun K, Wang S, Cao Y. Square-root unscented Kalman filter for ammonia coverage ratio and input ammonia estimations in diesel-engine urea-SCR system. ISA Trans 2020;96:299–308. http://dx.doi.org/10.1016/j.isatra.2019.06.025.
[25] Skaf Z, Aliyev T, Shead L, Steffen T. The state of the art in selective catalytic reduction control. In: SAE technical papers. SAE International; 2014, http://dx.doi.org/10.4271/2014-01-1533.
[26] Mora Pérez J. Control-oriented modelling and diagnostics of diesel after-treatment catalysts (Ph.D. thesis), Valencia (Spain): Universitat Politècnica de València; 2018, http://dx.doi.org/10.4995/Thesis/10251/115937.
[27] Ebrahimi M, Najafi M, Jazayeri SA. Multi-input–multi-output optimization of reactivity-controlled compression-ignition combustion in a heavy-duty diesel engine running on natural gas/diesel fuel. Int J Engine Res 2020;21:470–83. http://dx.doi.org/10.1177/1468087419832085.
[28] Mohanasundaram N. Non linear predictive modelling for IC engine using artificial neural network. In: 2020 fourth international conference on I-SMAC (IoT in social, mobile, analytics and cloud) (I-SMAC). IEEE; 2020, p. 801–7. http://dx.doi.org/10.1109/I-SMAC49090.2020.9243342.
[29] Childress B, Chen P. A decomposition algorithm for a class of nonlinear dynamic systems with cross-sensitive output measurement. In: 2018 IEEE conference on decision and control (CDC). IEEE; 2018, p. 662–7. http://dx.doi.org/10.1109/CDC.2018.8619701.
[30] Pla B, Piqueras P, Bares P, Aronis A. Simultaneous NOx and NH3 slip prediction in a SCR catalyst under real driving conditions including potential urea injection failures. Int J Engine Res 2021. http://dx.doi.org/10.1177/14680874211007646.
[31] Singalandapuram Mahadevan B, Johnson JH, Shahbakhti M. Development of a Kalman filter estimator for simulation and control of particulate matter distribution of a diesel catalyzed particulate filter. Int J Engine Res 2020;21:866–84. http://dx.doi.org/10.1177/1468087418785855.
[32] Jiang K, Yan F, Zhang H. Hydrothermal aging factor estimation for two-cell diesel-engine scr systems via a dual time-scale unscented Kalman filter. IEEE Trans Ind Electron 2020;67(1):442–50. http://dx.doi.org/10.1109/TIE.2019.2896030.
[33] Wang L. Model predictive control system design and implementation using MATLAB®. Advances in industrial control, London: Springer London; 2009.